Title

Synthesis and characterization of Pt(Cu0.67Sn0.33)

Authors

Juarez-Arellano, EA

Schellhase, S

Morgenroth, W

et al.

Publication Date

2020-07-01

DOI

10.1016/j.solidstatesciences.2020.106282

Peer reviewed

Synthesis and characterization of $Pt(Cu_{0.67}Sn_{0.33})$

E. A. Juarez-Arellano [a,b], S. Schellhase [a], W. Morgenroth [a], J. Binck [a], N. Tamura [c], C. Stan [c], D. Spahr [a], L. Bayarjargal [a], A. Barkov [d], V. Milman [e], A.-C. Dippel [f], M. v. Zimmermann [f], O. Ivashko [f], O. Gutowski [f], B. Winkler [a]

[a] *Institut für Geowissenschaften, Kristallographie/Mineralogie, Goethe-Universität Frankfurt, Altenhöferallee 1, D-60438 Frankfurt a.M., Germany.*

[b] *Universidad del Papaloapan, Circuito Central 200, Parque Industrial, 68301 Tuxtepec, Oaxaca, México.*

[c] *ALS, Lawrence Berkeley National Laboratory, Berkeley, CA 94720, USA.*

[d] *Research Laboratory for Industrial and Ore Mineralogy, Cherepovets State University, Cherepovets, Russia.*

[e] *Dassault Systèmes BIOVIA, Cambridge, United Kingdom.*

[f] *Deutsches Elektronen-Synchrotron, Notkestr. 85, 22607, Hamburg, Germany*

Abstract

$Pt(Cu_{0.67}Sn_{0.33})$ has recently been found in a natural sample. In order to be able to characterize this new ternary compound, we synthesized it from the elements. Samples were characterized by X-ray powder diffraction, differential scanning calorimetry, thermal relaxation calorimetry, and scanning electron microscopy studies. Density functional theory-based model calculations complemented the ex-

perimental studies. Pt($Cu_{0.67}Sn_{0.33}$) was already formed at a relatively low temperature of 773 K. Rietveld refinement of Pt($Cu_{0.67}Sn_{0.33}$) has been carried out in space group $P4/mmm$, with Pt on 0,0,0 and disordered Cu and Sn on $\frac{1}{2},\frac{1}{2},\frac{1}{2}$ and $Z = 1$. The lattice parameters are $a = 2.82205(1)$ Å, $c = 3.63637(2)$ Å, and $V = 28.9599(2)$ Å^3; which are in good agreement with values obtained earlier on the natural sample and with the results of DFT calculations. The standard entropy for Pt($Cu_{0.67}Sn_{0.33}$) is $S^{\circ}_{298.15} = 79.9(7)$ J mol^{-1}K^{-1}. The pressure dependence up to 36(2) GPa of the unit-cell volume and the lattice parameters and unit-cell volume have been obtained by synchrotron based powder diffraction using a diamond anvil cell. A fit of a 3rd-order Birch-Murnaghan equation of state to the Pt($Cu_{0.67}Sn_{0.33}$) (p, V)-data results in a bulk modulus of $B_0 = 215(27)$ GPa and $B' = 5(2)$.

Key words: Pt($Cu_{0.67}Sn_{0.33}$), ternary Pt-Cu-Sn compound, compressibility

1 Introduction

Binary Pt-Sn, Pt-Cu and Cu-Sn alloys are well known and have extensively been studied. The Cu-Sn system includes bronze alloys and phases used as solder such as Cu_5Sn_6 (Fürtauer et al. 2013). In the Pt-Sn system, PtSn and Pt_3Sn are used as catalysts for ethanol electrooxidation (Chia and Lee 2010). The family of ternary Pt-Cu-X, Pt-Sn-X and Cu-Sn-X alloys contains several hundred compounds. Among them, nine isostructural families of compounds can be identified, six with rare earth (R) elements (RCuSn$_2$ - $Cmcm$, RCu$_2$Sn$_2$ - $P4/nmm$, R_3Cu$_4$Sn$_4$ - $Immm$, RCuSn - $P6_3mc$, RCuSn - $P6_3/mmc$, RPtSn - $Pnma$, RPtSn - $P\bar{6}2m$) and two with $3d$ transition metal elements (M) (MCu$_2$Sn - $Fm\bar{3}m$, MPtSn - $F\bar{4}3m$) (Hellenbrandt 2004). However, no Pt-Cu-Sn ternary compound had been reported until very recently, when a mineral grain with approximate composition Pt($Cu_{0.67}Sn_{0.33}$) was discovered in an

ore from the Bolshoy Khailyk placer deposit, Eastern Sayans in the east of Russia (Barkov et al. 2018). After an initial characterization of this grain by Laue microdiffraction at the Advanced Light Source, Berkeley (beam line 12.3.2) by us, a request to register this new phase as a new mineral species has been submitted. As this mineral is exceedingly rare, we synthesized this ternary Pt-Cu-Sn compound in order to provide sample material for more detailed studies of its structure, stability and physical properties. Syntheses have been carried out by heating mixtures of the elements in a furnace and in an electric arc melter. Samples were characterized by X-ray powder diffraction, differential scanning calorimetry (DSC), thermal relaxation calorimetry, and scanning electron microscopy studies. Density functional theory-based model calculations complemented the experimental studies.

2 Experimental

2.1 Synthesis

$Pt(Cu_{0.67}Sn_{0.33})$ was synthesized by heating stoichiometric mixtures of analytical grade powders of platinum (0.2-1.8 μm, ChemPUR 99.95%), copper (<150 μm, ChemPUR 99.99%) and β-tin (<71 μm, MERCK 99%). Powders of platinum, copper and tin in a molar ratio of 3:2:1 were homogenized in an agate mortar and pressed into pellets of 4 mm diameter. In order to avoid oxidation, the pellets were placed in silica glass tubes, which were flushed three times with argon before sealing. As it had been reported earlier that β-Sn nucleation is a key step in the formation of Sn-based compounds (Ma et al. 2018), we have employed a variety of synthesis conditions in a conven-

tional oven starting at low temperature when investigating the formation of $Pt(Cu_{0.67}Sn_{0.33})$ (Tables 1 and 2). Based on results of DSC measurements (see below) a heating rate of 6 K/min was selected for all syntheses. In one set of experiments the furnace was switched off after holding the temperature at the maximum temperature, and the pellets were cooled down in the furnace to ambient conditions within several hours. In a second set of experiments, the pellets were quenched to ambient temperature in less than one minute using compressed air. It is worth noting that the temperatures explored in this study are rather low, as the melting point of platinum is ∼2041 K (Bezemer and Jongerius 1976).

$Pt(Cu_{0.67}Sn_{0.33})$ was also synthesized in an arc-melter (MAM-1, E. Bühler GmbH, Hechingen) by melting a stoichiometric mixture of the elements. Powders of the elements were mixed in an agate mortar and pressed into pellets of 4 mm diameter as described above. Prior to the arc melting experiments, the sample chamber was flushed three times with argon and remaining traces of oxygen were removed by melting a titanium sphere in the sample chamber. Temperatures in the arc melter are substantially higher than in the furnace (>2000 K as the melting point of Ti is exceeded). After the synthesis, the pellet rapidly (<1 min) reached ambient temperature after the arc is switched off.

2.2 Characterization

2.2.1 Powder diffraction

Powder X-ray diffraction patterns were collected at ambient temperature with a Panalytical Philips X'Pert diffractometer using the pellets without further sample preparation. $CuK_{\alpha 1}$ radiation from a Cu anode operating at 40 kV - 30 mA and a focusing Johansson Ge monochromator was used. Powder diffraction patterns were measured with a PIXcel^{3D} 2×2 detector. Instrumental parameters were obtained by measuring a Si-standard. Indexing was performed using the DICVOL program (Boultif and Louer 2004), while Le Bail fits and Rietveld refinement were performed using the program FULLPROF (Rodriguez-Carvajal 1993). A linear interpolation between approximately 30 manually selected points for the background and a pseudo-Voigt profile function were used.

2.2.2 Differential scanning calorimetry

Differential Scanning Calorimetry was carried out using small pellets of a stoichiometric mixture of elemental platinum, copper and tin powders in molar ratio of 3:2:1. To establish sufficient thermal contact between the alumina crucibles and the sample the mixtures were homogenized in an agate mortar and pressed into small pellets. Pellets of 10-20 mg of sample were placed in open alumina crucibles. A NETSCH DSC 204 F1 Phoenix instrument was used. Measurements were carried out with heating-cooling rates ranging from 1 K/min to 6 K/min in a helium atmosphere in the temperature range between 300 - 680 K.

2.2.3 Scanning electron microscopy

The morphology and characteristics of the surface of the samples were observed by Scanning Electron Microscopy using a Phenom World Pro X Desktop SEM microscope operating at 15 kV. Images were acquired using a BSE-detector. Semi-quantitative element identification was performed by X-ray energy dispersive spectroscopy (EDS) using an acceleration voltage of 15 kV. Several regions of the pellets were selected for the measurements.

2.2.4 Heat capacity measurements

The heat capacity measurements were performed at temperatures between 3.8 - 393 K using a relaxation calorimeter (Physical Properties Measurement System (PPMS), Quantum Design). A compacted, polycrystalline fragment with mass 14.98(2) mg was measured at 150 different temperatures. At each temperature, the heat capacity was measured three times by the relaxation method using the two-τ model. The temperature step was reduced logarithmically from 393 K to 3.8 K. The accuracy of our experiments was established by measuring the standard reference materials SRM-720 (Al_2O_3) and Cu (Alfa Aesar, 99.999%). The deviation of our data for SRM-720 from to those published by Ditmars et al. (1982) was within 2% in the range of 395 K to 50 K and was within 6% below 5 K. The deviation of our data for Cu from those reported by Lashley et al. (2003) was 1% in the range from 300 K to 40 K, and 2% below 40 K. The standard molar entropy $S^{\circ}_{298.15}$ and the enthalpy change in between 0–298.15 K, $\triangle H_{0-298.15}$, were computed with the following equations:

$$S^{\circ}_{298.15} = \int_{0}^{298.15} \frac{C_p}{T} dT \tag{1}$$

and

$$\triangle H_{0-298.15} = \int_{0}^{298.15} C_p dT \tag{2}$$

Neglecting the difference between C_p and C_V at lower temperatures, the Debye temperature θ_D can be determined using

$$C_V = \frac{12\pi^4}{5} nR\left(\frac{T^3}{\theta_D}\right) \tag{3}$$

where n is the number of atoms per unit cell and $R = 8.31446$ J mol^{-1}K^{-1} (Hunklinger 2009).

2.2.5 High energy synchrotron diffraction experiments

Powder diffraction patterns were collected at the High Energy Diffraction Beamline P21.1 (PETRA III, DESY, Hamburg, Germany) on pellets reacted according to the temperature profile S5 described in Table 2. The diameters of the pellets were 2 and 4 mm. Diffraction patterns were acquired using a wavelength of 0.1204 Å and a PerkinElmer XRD 1621 detector. The beam size was 1000 × 500 μm (H × V). The sample-to-detector distance of 1353.5 mm and the wavelength were determined employing a Ni reference sample. All the diffraction data were processed with the Dioptas software (Prescher and Prakapenka 2015).

2.2.6 High pressure diffraction experiments

High pressure experiments using diamond anvil cells were carried out at the Extreme Conditions Beamline P02.2 (PETRA III, DESY, Hamburg, Germany) (Liermann et al. 2010). A $10 \times 15 \times 5$ μm^3 fragment of a Pt($Cu_{0.67}Sn_{0.33}$)

from the S4 synthesis (Table 2) was loaded into a Boehler-Almax type diamond anvil cell (DAC) (Boehler 2006) for the high pressure experiment. A ruby chip was loaded and the pressure was determined using the ruby fluorescence method (Mao et al. 1978; 1986). Ne was employed as a pressure-transmitting medium. The sample was placed in a 175 μm diameter hole which was drilled by a custom-built laser lathe in a pre-indented Re gasket (45 μm in thickness). The diamond culets had a 350 μm diameter and an opening angle of 70°. Diffraction patterns were acquired using a wavelength of 0.2893 Å, a beam focused to 9×3 μm^2 (H $\times$ V) full width at half maximum using compound reflective lenses, and a PerkinElmer XRD1621 flat panel detector. The sample-to-detector distance of 395.71 mm and the wavelength were determined employing a CeO_2 reference sample. Measurement times were 10 s, during which the samples were rotated by $\pm$ 10° around an axis perpendicular to the beam. All the diffraction data were processed with the Dioptas software (Prescher and Prakapenka 2015). Powder diffraction data were collected from ambient pressure up to 36(2) GPa. Lattice parameters have been obtained from Le Bail fits using GSAS/EXPGUI (Toby 2001). The bulk modulus was derived using the EoSFit7 program (Gonzalez-Platas et al. 2016).

3 Density functional theory

Density functional theory (DFT) calculations were performed using the CASTEP code (Clark et al. 2005). The code is an implementation of Kohn-Sham DFT based on a plane wave basis set in conjunction with pseudopotentials. The plane-wave basis set is unbiased (as it is not atom-centered) and does not suffer from the problem of basis-set superposition error unlike atom-centered

basis sets. It also makes converged results straightforward to obtain in practice, as the convergence is controlled by a single adjustable parameter, the plane wave cut-off, which we set to 450 eV. All pseudopotentials were ultrasoft, and were generated using the PBE exchange-correlation functional (Perdew et al. 1996) using the 'on the fly' parameters included in the CASTEP distribution. The Brillouin-zone integrals were performed using Monkhorst-Pack grids (Monkhorst and Pack 1976) with spacings between grid points of less than 0.02 $Å^{-1}$. Full geometry optimizations of the unit cell parameters and the internal coordinates were performed until forces were converged to <0.01 eV/Å and the residual stress was <0.02 GPa.

As CASTEP employs periodic boundary conditions, the Cu-Sn disorder was approximated, first by carrying out calculations in a $3 \times 3 \times 3$ supercell in space group $P1$ containing 27 formula units with random exchange of Sn and Cu. A further set of calculations were carried out in a supercell where the Sn and Cu atoms were exchanged to give a "special quasi-random structure" (Zunger et al. 1990). The special Quasirandom Structure (SQS) was generated using the method suggested by van de Walle et al. (2013). The algorithm searches for the best periodic approximation to the true disordered state for a given number of atoms per supercell. The method is based on Monte Carlo simulated annealing iterations with an objective function that seeks to match the maximum number of correlation functions.

4 Results and Discussion

4.1 Differential Scanning Calorimetry

The onset of a reaction in the mixture of the elements is clearly observable by DSC (Figure 1). At 500 K, superposed on the broad endothermic signal

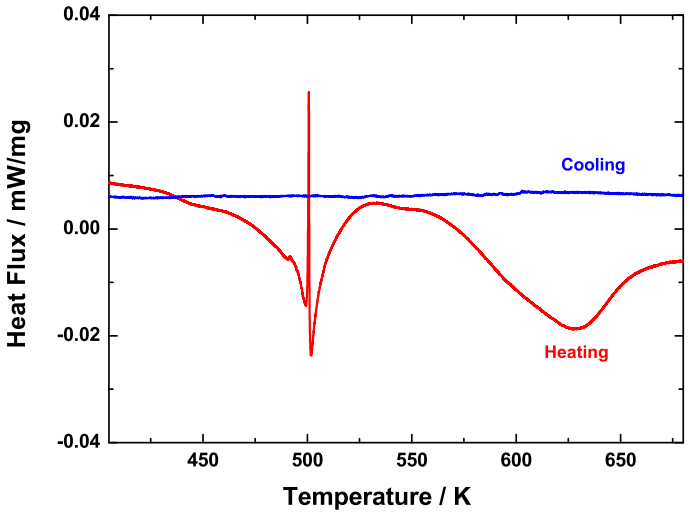

Fig. 1. Differential scanning calorimetry curve of a stoichiometric mixture of elemental platinum, copper and tin powders in molar ratio of 3:2:1 heated and cooled with 6 K/min.

associated with the melting of tin (T_{melt}(Sn)∼503 K (Jiang et al. 2006)) a very narrow exothermic signal appears. Loomans and Fine (2000) reported a similar behaviour in Ag-Cu-Sn ternary alloys which they associated with the formation of a non-eutectic intermetallic alloy. In contrast to the observations by Loomans and Fine (2000), where the exothermic signal is just above the background level, in this study the magnitude of the exothermic heat flux is considerably larger. The associated chemical reaction is irreversible, as there is no corresponding signal in the flat DSC curve obtained on cooling. No

significant change other than an increase in the data scatter in the heat flow is observed if the heating rate is decreased to 1 K/min.

4.2 Powder diffraction at ambient conditions

The powder diffraction patterns from the mixture of the elements, after homogenization in the mortar, and from the products of the synthesis can be seen in Figures 2 and 3.

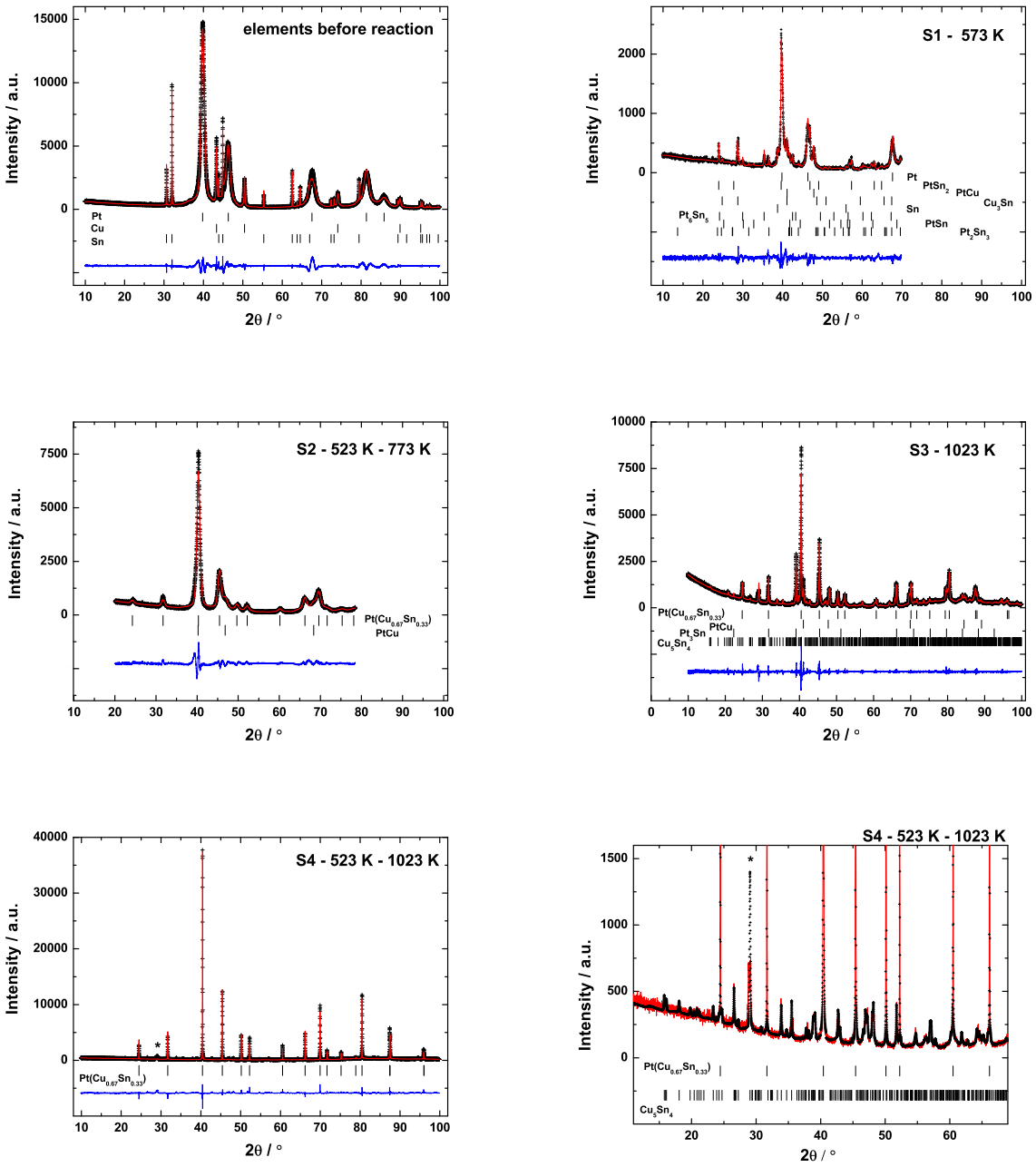

Fig. 2. Le Bail fitting of X-ray powder diffraction patterns using $\lambda = 1.5406$ Åof Pt-Cu-Sn (3:2:1) before the reaction and after different synthesis routes (S1, S2, S3 and S4), see Tables 1 and 2. The asterix in the diffractogram from the S4 synthesis highlights the most intense reflection of the secondary η'-Cu_5Sn_4 phase.

The lattice parameters of the obtained phases are shown in Tables 1 and 2.

The diffraction pattern from the Pt-Cu-Sn starting mixture shows narrow reflections from copper and β-tin but broad reflections from platinum. This difference is due to the variation in particle size (Pt: 0.2-1.8 μm, Cu: <150 μm, and β-tin: <71 μm).

The maximum temperature (T_{max}(S1) = 573 K) in synthesis S1 was above the exothermic reaction observed by DSC. The diffraction pattern shows that the elements partially reacted, but after cooling only binary compounds were present (Table 1). Platinum remains partially unreacted at these conditions. This synthesis clearly shows the complexity of reactions in the Pt-Cu-Sn system, as the formation of $PtSn_2$, PtCu, Cu_3Sn, Cu_6Sn_5, PtSn and Pt_2Sn_3 is observed. The lattice parameters obtained for those compounds agree with those reported earlier (Table 1).

In synthesis S2, the temperature is first raised slightly above the exothermic reaction and then increased to a nominal temperature of 773 K. At these conditions Pt($Cu_{0.67}Sn_{0.33}$) was obtained, although not as a pure phase as it is accompanied by moderate amounts of PtCu (Table 2). The diffraction peaks are unusually broad in samples obtained when using these conditions. X-ray diffraction peaks noticeably broaden either when crystallites become smaller than about a micrometer or if the lattice is strained, e.g. due to an abundance of defects (Ungár 2004). Because the pellet was cooled down slowly in the furnace, broadening due to lattice strains seems unlikely. If broadening is due to crystallite size, then this implies that at 773 K the Pt($Cu_{0.67}Sn_{0.33}$) phase is just starting to be formed. It is worth mentioning that the synthesis of this Pt-based compound is achieved at around one third of the melting temperature of platinum. This is considerably lower than the formation temperatures reported for binary Pt-based alloys (e.g. $PtSn_2$ ~1000 K, PtCu ~1100 K, PtSn ~1170

K, or Pt_3Sn ~1370 K (Anres et al. 1998, Abe et al. 2006)).

In synthesis S3 the maximum temperature was 1023 K. At these conditions the formation of $Pt(Cu_{0.67}Sn_{0.33})$ could also be observed. However, considerable amounts of PtCu, Pt_3Sn and η'-Cu_5Sn_4 are also present. At this temperature the reflections of $Pt(Cu_{0.67}Sn_{0.33})$ are sharp and intense, which indicates that the crystallinity is much improved in comparison to the sample obtained at 773 K.

It has been reported that solid state diffusion controls the growth of phases in Sn-based systems (Baheti et al. 2018). Therefore, in order to promote diffusion, in synthesis S4 we first heated the sample to a temperature slightly above the exothermic reaction, maintained this temperature for 5 h, and then increased the temperature to 1023 K. This procedure leads to the formation of almost pure $Pt(Cu_{0.67}Sn_{0.33})$ (Table 2, Figure 2). The S4 synthesis contained a small amount of a secondary phase, which has been tentatively assigned as η'-Cu_5Sn_4 (Figure 2). The lattice parameters obtained by a Le Bail fit (Table 2) are similar to those reported by Larsson et al. (1994). Several attempts with slight changes of the stoichiometry were carried out in order to investigate if this could lead to the formation of a single $Pt(Cu_{0.67}Sn_{0.33})$ phase, but a secondary phase was always observed. However, the amount of η'-Cu_5Sn_4 in the pellet is so small that it was impossible to perform a reliable Rietveld refinement of this phase and establish its concentration.

Synthesis S5 was done using the same temperature profile as in S4, but the pellet was quenched using compressed air instead of cooling it down slowly in the furnace to ambient conditions within several hours. This procedure leads to the formation of pure $Pt(Cu_{0.67}Sn_{0.33})$, independent of the pellet diameter,

where diameters of 2 and 4 mm were employed (Figure 3, Table 2).

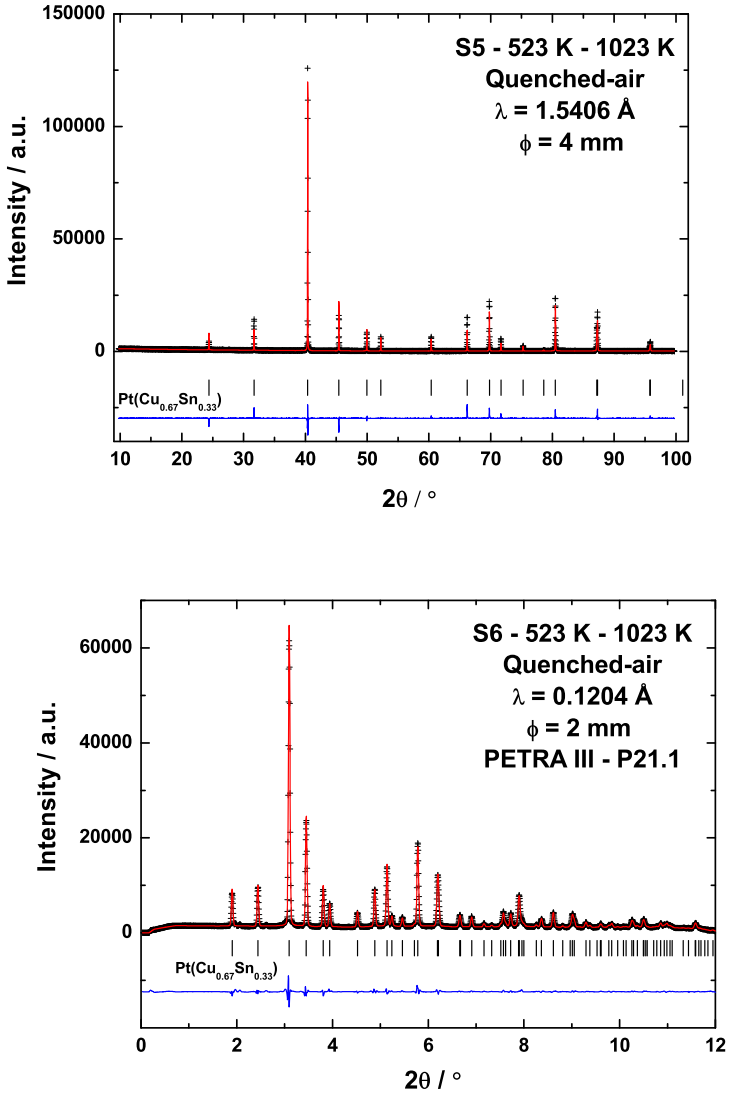

Fig. 3. Rietveld refinements of $Pt(Cu_{0.67}Sn_{0.33})$ obtained by a two stage synthesis in which the samples were temperature-quenched with compressed air (Table 2, syntheses S5 and S6).

4.3 Arc-Melting synthesis

$Pt(Cu_{0.67}Sn_{0.33})$ was also synthesized in an arc-melter by melting the elements (S7). The Le Bail fit of the powder diffraction pattern of $Pt(Cu_{0.67}Sn_{0.33})$ from the arc-melter is shown in Figure 4. The lattice parameters are listed in Table 3. The reflections from the sample obtained by arc-melting are broad. As mentioned above, the broadening can be associated to small crystallites or strains (Ungár 2004). The pellet in the arc-melter was heated and quenched much faster than in the furnace-based experiments and hence both the presence of small crystallites and strains are to be expected. The arc-melter synthesis produced two other phases: cubic $Pt_{0.9}Cu_{0.1}$ (Table 3) and a further phase that could not be identified due to the strong broadening of the reflections of the main phase and the significant overlap of reflections.

In order to release strains and to evaluate the thermal stability of $Pt(Cu_{0.67}Sn_{0.33})$ obtained by arc-melting, the sample was heat treated. First, the temperature was increased from ambient consitions to 973 K with a rate of 1.3 K/min. The sample was then kept at this temperature for 144 h. Afterwards, the sample was cooled down to ambient conditions in the furnace within 12 h (Table 2 synthesis S7-annealed). The unidentified reflections observed in synthesis S7 disappeared while reflections due to $Pt_{0.9}Cu_{0.1}$ remained after annealing (Figure 4). The diffraction pattern of the annealed $Pt(Cu_{0.67}Sn_{0.33})$ sample shows sharp reflections, but all of them show peak splitting. The best Le Bail fitting was achieved using three different unit cells, two cells with space group $P4/mmm$ and one with $Pmmm$ (Table 3, Figure 4). The peak splitting and the loss of symmetry is very likely related to short-range order such as the one observed in other Cu-based compounds (Tsatskis and Salje 1998, Wolverton

et al. 1998).

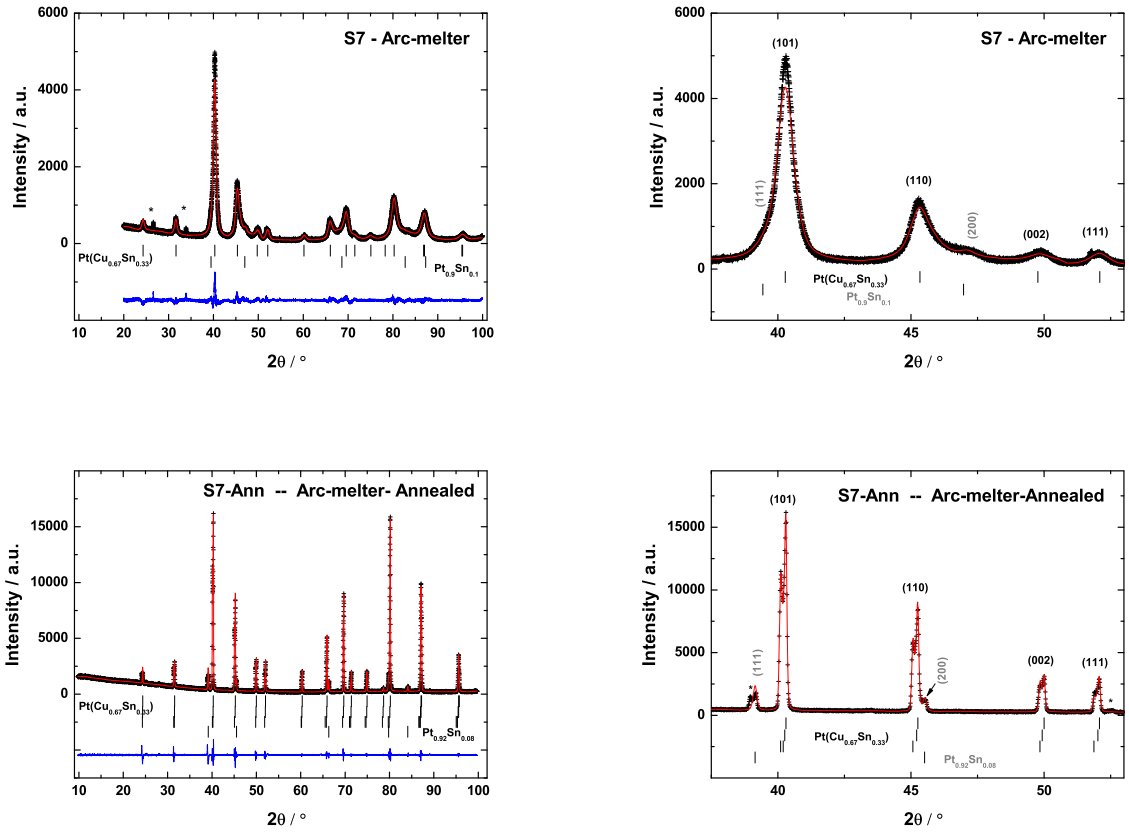

Fig. 4. Le Bail fits of $Pt(Cu_{0.67}Sn_{0.33})$ synthesized in an arc-melter by melting the elements (synthesis S7, table 2) and after annealing the pellet at 973 K for 144 h ((synthesis S7-annealed, table 2)). $Pt_{0.9}Cu_{0.1}$ was identified as a secondary phase. Unidentified reflections are highlighted with asterixs.

4.4 Microstructures

The synthesis products have been characterized by scanning electron microscopy. Representative images are shown in Figure 5. In general, the mi-

crostructure observed in the SEM images can be related to the phases identified in the diffraction patterns (Figures 2 and 4, Tables 1, 2 and 3). Several phases can be observed in the samples from the synthesis S1 and S3 (Figure 5-a,c) while only two phases are detectable in syntheses S2 and S4 (Figure 5-b,d). Figure 5-d shows a homogeneous microstructure which, according to X-ray diffraction, corresponds to Pt($Cu_{0.67}Sn_{0.33}$).

(a) S1 – 573K

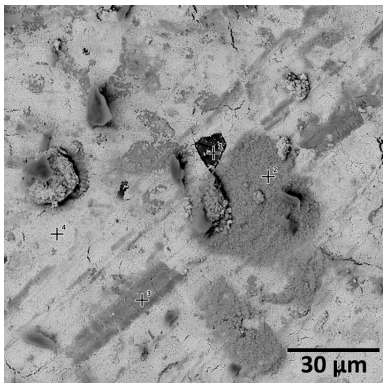

(b) S2 – 523K - 773 K

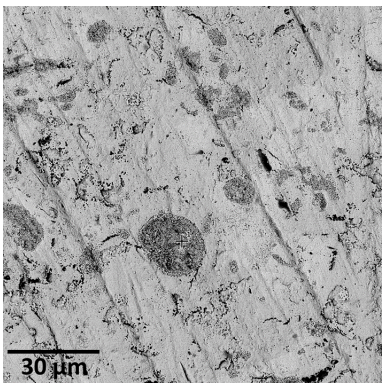

(c) S3 – 1023K

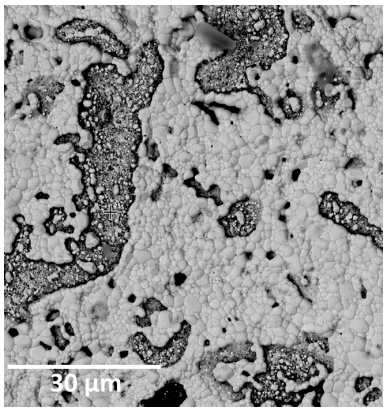

(d) S4 – 523K - 1023 K

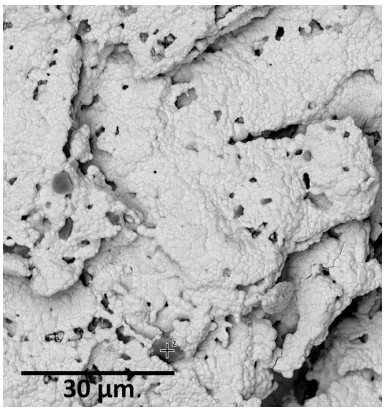

(e) S7 – Arc-melter

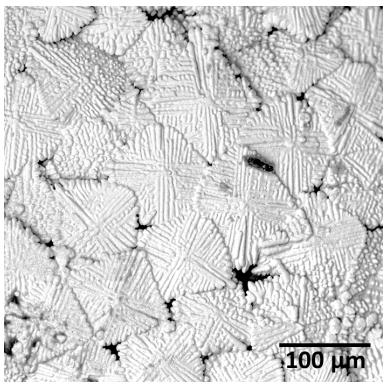

(f) S7 – Arc-melter

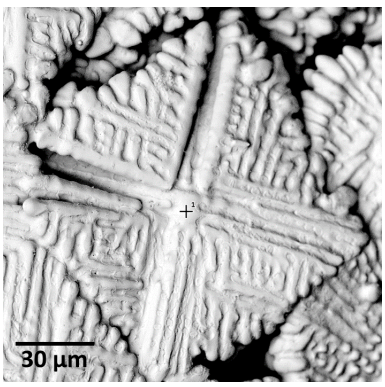

Fig. 5. Scanning electron micrographs of the microstructure of Pt-Cu-Sn (3:2:1) pellets after different synthesis routes in the furnace (S1, S2, S3 and S4) and in the arc-melter (S7).

The pellet synthesized by arc-melting shows a homogeneous dendritic microstructure (Figure 5-e,f). During the arc-melter synthesis, the heating and cooling rates are fast, with $(dT/dt) \sim 2000$ K/min. Such large cooling rates lead to a homogeneous nucleation in the melt (Kurz and Fisher 1998). In single-phase alloys, the nuclei grow into primary crystals which rapidly become unstable and transform to dendritic form. These dendrites grow freely in the melt in an equiaxial shape because their latent heat is extracted radially through the undercooled melt and they finally impinge on one another (Kurz and Fisher 1998). EDX analysis from several regions of the pellets gives an approximate composition of $PtCu_{0.7(1)}Sn_{0.3(1)}$ which is in satisfactory agreement with the nominal $Pt(Cu_{0.67}Sn_{0.33})$ stoichiometry.

4.5 Pt($Cu_{0.67}Sn_{0.33}$) crystal structure

The unit cell of $Pt(Cu_{0.67}Sn_{0.33})$ was determined from the S5 and S6 powder diffraction patterns using the DICVOL program. The Rietveld method as implemented in the FULLPROF program was used to refine the crystal structure. The results of the Rietveld refinements for $Pt(Cu_{0.67}Sn_{0.33})$ are shown in Figure 3. The lattice parameters, the atomic parameters and the reliability factors are given in Tables 4 and 5. Refinements of the site occupancies give an approximate composition of $Pt(Cu_{0.59(5)}Sn_{0.41(5)})$, which is in very good agreement with the nominal $Pt(Cu_{0.67}Sn_{0.33})$ stoichiometry.

The crystal structure of the $Pt(Cu_{0.67}Sn_{0.33})$ compound is shown in Figure 6.

It is a tetragonal distorted CsCl-type structure, space group $P4/mmm$, in which Cu and Sn occupy the same Wyckoff position (1d). The results from the annealed arc-melter sample imply that annealing leads to short-range order in the structure, but this needs to be further explored.

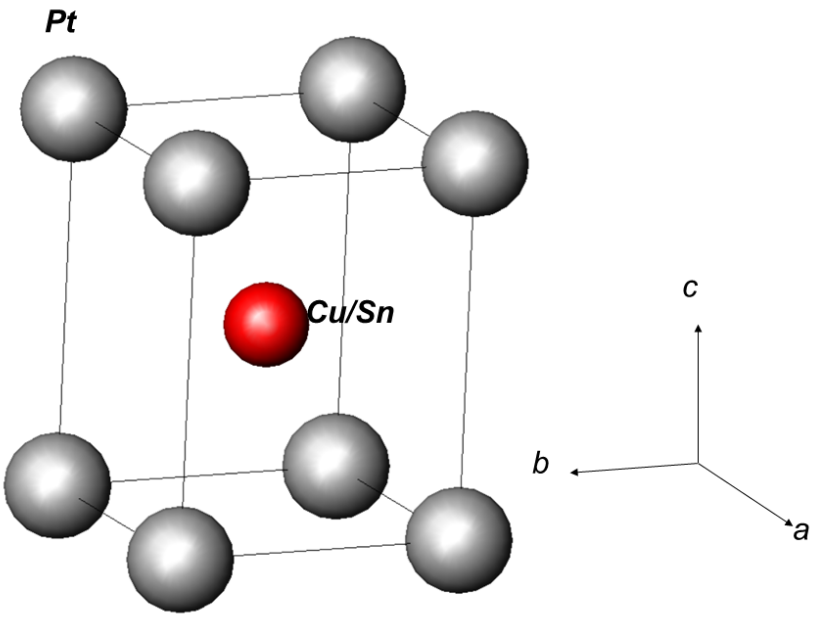

Fig. 6. Crystal structure of $Pt(Cu_{0.67}Sn_{0.33})$ obtained by Rietveld refinement. Pt-atoms are depicted as gray spheres while Cu/Sn atoms are shown as red spheres.

4.6 Heat capacity

Figure 7 shows the heat capacity of $Pt(Cu_{0.67}Sn_{0.33})$ (pellet from S5) between 3.8 and 393 K, while the T^3-plots are shown in Figure 8. The heat capacity

is 54.3(6) J $mol^{-1}K^{-1}$ at 298.15 K. The data was fitted by fifth-order polynomial functions in three temperature ranges. Polynomial coefficients are given in Table 6. The data implies that there is no structural or magnetic phase transition at ambient pressure between 3.8 K and 400 K.

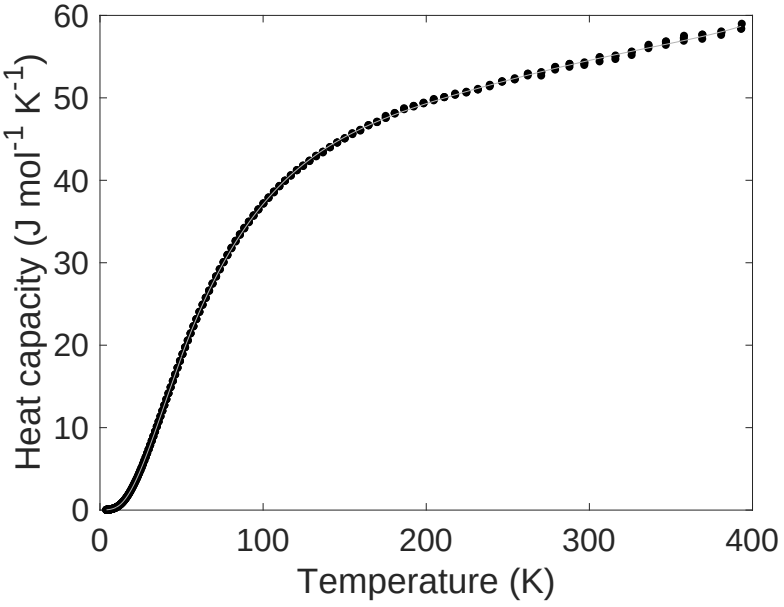

Fig. 7. The heat capacity of $Pt(Cu_{0.67}Sn_{0.33})$ (synthesis S5 Tab. 2) measured between 3.8 and 393 K. Experimental data are shown as dots, the continuous curve is the result of a polynomial fit.

The Debye temperature of $Pt(Cu_{0.67}Sn_{0.33})$ was determined using eq. 3 and is $\theta_D = 221(4)$ K. It is in similar to the Debye temperatures of elemental platinum (236(2) K(Arblaster 1994)) and tin (200(3) K (Bryant and Keesom 1961)), but smaller than the Debye temperature of copper (342-345 K(Arblaster 2015)).

The standard entropy for $Pt(Cu_{0.67}Sn_{0.33})$ is $S^{\circ}_{298.15} = 79.9(7)$ J $mol^{-1}K^{-1}$ and hence is very closs to the concentration-weighted sum of the pure elements (Pt: 41.53 J $mol^{-1}K^{-1}$ (Arblaster 1994), Cu: 33.1 J $mol^{-1}K^{-1}$, (Arblaster 2015) α-Sn: 44.14(42) and β-Sn: 51.18(08) (Gamsjäger et al. 2012)).

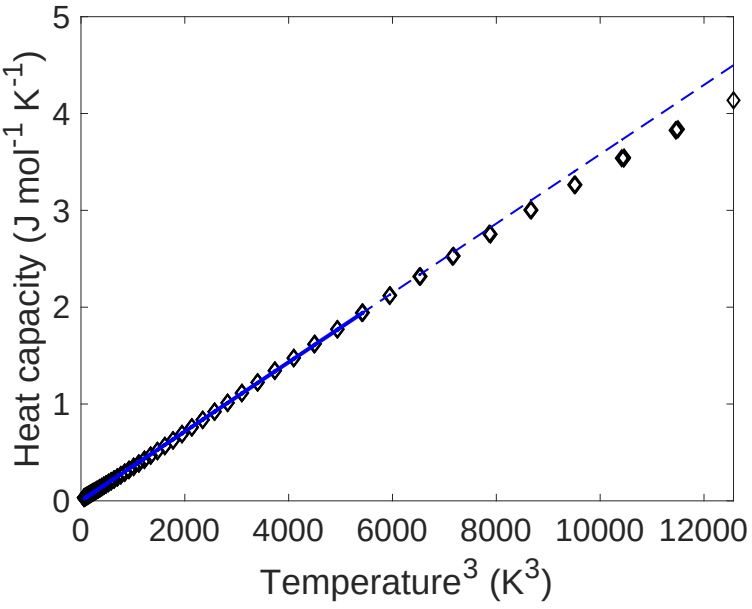

Fig. 8. T3-fit of $Pt(Cu_{0.67}Sn_{0.33})$ (S5) is represented by the solid line. The dashed line represents the extrapolation of the fit.

The enthalpy, $H^{\circ}_{298.15}$-H°_{0}, for $Pt(Cu_{0.67}Sn_{0.33})$ at 298 K is H = 11.345 (kJ mol^{-1}) and thus close to the concentation-weighted sum of the values for the elements (Pt: 5.694 kJ mol^{-1} (Arblaster 1994), Cu: 5.003 kJ mol^{-1} (Arblaster 2015), and Sn: 6.316 kJ mol^{-1} (Khvan et al. 2019)).

4.7 Pt($Cu_{0.67}Sn_{0.33}$) compressibility

The equation of state of $Pt(Cu_{0.67}Sn_{0.33})$ has been obtained up to a pressure of 36(2) GPa. The bulk modulus obtained from fits of 2^{nd} and 3^{rd}-order Birch-Murnaghan equations of state to the experimental data and to the results of the DFT calculations are given in Figure 9 and Tables 7 and 8. The compression behavior of the lattice parameters is also shown in Figure 9. The experi-

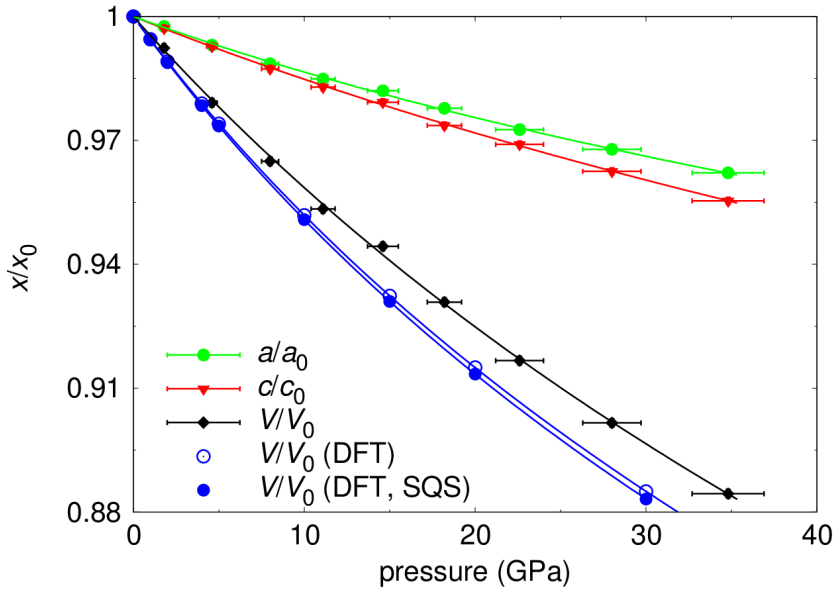

Fig. 9. Pressure dependence of lattice parameters from experiment (synthesis S4) and DFT of $Pt(Cu_{0.67}Sn_{0.33})$ up to 36 GPa, and fits of third order Birch-Murnaghan equations of state to the data. The open circles represent DFT data from a $3 \times 3 \times 3$ supercell in which Cu and Sn atoms have been exchanged randomly, while the solid circles are results for a 54 atom special quasi-random structure. The experimental bulk modulus is 215(3) GPa with a $B' = 5(2)$, while the theoretical bulk moduli are 191(2) GPa for the "random" structure and 173.6(2) GPa for the SQS structure.

mental bulk modulus is $\approx$ 220 GPa, depending on which equation of state is employed. A fit to the DFT results are slightly lower (174 - 200 GPa), which is due to the often observed underbinding in DFT-GGA-PBE calculations. The c-axis is more compressible than the a-axis, which is the expected behavior as the c-axis is longer and hence interatomic distances along [001] are larger than in the (001) plane. No pressure-induced structural phase transition has been observed upon pressure increase in the pressure range sampled here. The results show that $Pt(Cu_{0.67}Sn_{0.33})$ is more compressible than platinum (276 GPa), but less compressible than copper (138 GPa) or β-tin (52.8 GPa) (Li and Wu 2001). There are no readily available bulk moduli for binary Pt-Cu,

Pt-Sn and Cu-Sn compounds. However, the compressibility of $Pt(Cu_{0.67}Sn_{0.33})$ is similar to those of CoPt and NiPt alloys (∼220 GPa) (Shen et al. 2013). The two DFT calculations with different distributions of the Cu and Sn atoms give similar bulk moduli, thus showing that the bulk modulus is essentially independent of the local atomic arrangement in this compound.

5 Conclusion

The successful synthesis of a novel compound in the Pt-Cu-Sn system has allowed us to obtain physical and thermodynamic parameters, which will help to better understand the formation of this extremely rare mineral in nature. The peak splitting observed when quickly cooled samples were annealed points toward the tendency of the (Cu,Sn)-sublattice to order, but the exploration of this was beyond the scope of the present study. Finally, we have begun to use this compound as a base to derive single phase high entropy alloys by substitution on the sub-lattices and these results will be reported elsewhere.

6 Acknowledgments

This research was supported by Deutsche Forschungsgemeinschaft (Project Wi-1232 and DFG FOR 2125 “CarboPaT”) and from the German BMBF (project 05K16RFB). EAJA thanks Frankfurt University for financial support. The Advanced Light Source is supported by the Director, Office of Science, Office of Basic Energy Science, of the U.S. Department of Energy under contract DE-AC02-05CH11231. We are grateful to PETRA III at DESY (Hamburg, Germany), a member of the Helmholtz Association (HGF). We

would like to thank Hanns-Peter Liermann and his team for assistance in using beamline P02.2. Also, we are grateful for support by BIOVIA through the BIOVIA Science Ambassador program.

References

S. Fürtauer, D. Li, D. Cupid, H. Flandorfer, The Cu-Sn phase diagram, part I: New experimental results., Intermetallics 34 (2013) 142–147.

Z. W. Chia, J. Y. Lee, Direct ethanol fuel cells, in: R. H. Crabtree (Ed.), Energy Production and Storage. Inorganic Chemical Strategies for a Warming World, Wiley, 2010, pp. 229–250.

M. Hellenbrandt, The Inorganic Crystal Structure Database (ICSD) - Present and Future, Crystallography Reviews 10 (1) (2004) 17–22.

A. Y. Barkov, G. Shvedov, S. Silyanov, R. F. Martin, Mineralogy of Platinum-Group Elements and Gold in the Ophiolite-Related Placer of the River Bolshoy Khailyk, Western Sayans, Russia, Minerals 8 (6) (2018) 247.

Z. L. Ma, J. W. Xian, S. A. Belyakov, C. M. Gourlay, Nucleation and twinning in tin droplet solidification on single crystal intermetallic compounds, Acta Materialia 150 (2018) 281–294.

J. Bezemer, R. T. Jongerius, The melting temperature of platinum measured from continually melting and freezing ribbons, Physica C 83 (1976) 338–346.

A. Boultif, D. Louer, Powder pattern indexing with the dichotomy method, Journal of Applied Crystallography 37 (2004) 724–731.

J. Rodriguez-Carvajal, Recent advances in magnetic structure determination by neutron powder diffraction, Physica B 192 (1993) 55–69.

D. Ditmars, S. Ishihara, S. Chang, G. Bernstein, E. West, Enthalpy and heat-capacity standard reference material: synthetic sapphire (α-Al_2O_3) from 10

to 2250 K, J. Res. Natl. Bur. Stand 87 (2) (1982) 159–163.

J. Lashley, M. Hundley, A. Migliori, J. Sarrao, P. Pagliuso, T. Darling, M. Jaime, J. Cooley, W. Hults, L. Morales, et al., Critical examination of heat capacity measurements made on a Quantum Design physical property measurement system, Cryogenics 43 (6) (2003) 369–378.

S. Hunklinger, Festkörperphysik, Oldenbourg Verlag, 2009.

C. Prescher, V. B. Prakapenka, DIOPTAS: a program for reduction of two-dimensional X-ray diffraction data and data exploration, High Pressure Research 35 (2015) 223–230.

H. P. Liermann, W. Morgenroth, A. Ehnes, A. Berghäuser, B. Winkler, H. Franz, E. Weckert, The extreme conditions beamline at PETRA III, DESY: possibilities to conduct time resolved monochromatic diffraction experiments in dynamic and laser heated DAC, Journal of Physics: Conference Series 215 (2010) 012029.

R. Boehler, New diamond cell for single-crystal x-ray diffraction, Review of Scientific Instruments 77 (2006) 115103.

H. Mao, P. Bell, J. Shaner, D. Steinberg, Specific volume measurements of Cu, Mo, Pd, and Ag and calibration of the ruby R_1 fluorescence pressure gauge from 0.06 to 1 Mbar, Journal of Applied Physics 49 (1978) 3276–3283.

H. K. Mao, J. Xu, P. M. Bell, Calibration of the ruby pressure gauge to 800 kbar under quasihydrostatic conditions, JGR Solid Earth 91 (1986) 4673–4676.

B. H. Toby, EXPGUI, a graphical user interface for GSAS, Journal of Applied Crystallography 34 (2001) 210–213.

J. Gonzalez-Platas, M. Alvaro, F. Nestola, R. Angel, EosFit7-GUI: a new graphical user interface for equation of state calculations, analyses and teaching, Journal of Applied Crystallography 49 (2016) 1377–1382.

S. J. Clark, M. D. Segall, C. J. Pickard, P. J. Hasnip, M. J. Probert, K. Refson, M. C. Payne, First principles methods using CASTEP, Zeitschrift für Kristallographie 220 (2005) 567–570.

J. P. Perdew, K. Burke, M. Ernzerhof, Generalized gradient approximation made simple, Physical Review Letters 77 (1996) 3865–3868.

H. Monkhorst, J. D. Pack, Special points for Brillouin-zone integrations, Physical Review B 13 (1976) 5188–5192.

A. Zunger, S.-H. Wei, L. G. Ferreira, J. E. Bernard, Special quasirandom structures, Phys. Rev. Lett. 65 (1990) 353–356.

A. van de Walle, P. Tiwary, M. de Jong, D. L. Olmsted, M. Asta, A. Dick, D. Shin, Y. Wang, L.-Q. Chen, Z.-K. Liu, Efficient stochastic generation of special quasirandom structures, Calphad Journal 42 (2013) 13–18.

H. Jiang, K. Moon, H. Dong, F. Hua, C. P. Wong, Size-dependent melting properties of tin nanoparticles, Chemical Physics Letters 429 (2006) 492–496.

M. E. Loomans, M. E. Fine, Tin-Silver-Copper eutectic temperature and composition, Metallurgical and materials transactions A 31 (2000) 1155–1162.

T. Ungár, Microstructural parameters from X-ray diffraction peak broadening, Scripta Materialia 51 (2004) 777–781.

P. Anres, M. Gaune-Escard, J. P. Bros, E. Hayer, Enthalpy of formation of the (Pt-Sn) system, Journal of Alloys and Compounds 280 (1998) 158–167.

T. Abe, B. Sundman, H. Onodera, Thermodynamic assessment of the Cu-Pt system, Journal of Phase Equilibria and Diffusion 27 (2006) 5–13.

V. A. Baheti, S. Kashyap, P. Kumar, K. Chattopadhyay, A. Paul, Solid state diffusion-controlled growth of the phases in the Au-Sn system, Philosophical Magazine 98 (1) (2018) 20–36.

A. K. Larsson, L. Stenberg, S. Lidin, The superstructure of domain-twinned

η'-Cu_6Sn_5, Acta Crystallographica B 50 (1994) 636–643.

I. Tsatskis, E. K. H. Salje, Short-range order in a steady state of irradiated Cu-Pd alloys: comparison with fluctuations at thermal equilibrium, Journal of Physics: Condensed Matter 10 (1998) 3791–3806.

C. Wolverton, V. Ozolins, A. Zunger, First-principles theory of short-range order in size-mismatched metal alloys: Cu-Au, Cu-Ag, and Ni-Au, Physical Review B 57 (8) (1998) 4332–4348.

W. Kurz, D. J. Fisher, Fundamentals of Solidification, 4th Edition, CRC Press, 1998.

J. Arblaster, The thermodynamic properties of platinum on ITS-90, Platinum Metals Review 38 (3) (1994) 119–125.

C. Bryant, P. Keesom, Low-temperature specific heat of indium and tin, Physical Review 123 (2) (1961) 491.

J. W. Arblaster, Thermodynamic Properties of Copper, Journal of Phase Equilibria and Diffusion 36 (5) (2015) 422–444.

H. Gamsjäger, T. Gajda, J. Sangster, S. K. Saxena, W. Voigt, J. Perrone, Chemical Thermodynamics of Tin, Vol. 12 of Chemical Thermodynamics, Nuclear Energy Agency, 2012.

A. V. Khvan, T. Babkina, A. T. Dinsdale, I. A. Uspenskaya, I. V. Fartushna, A. I. Druzhinina, A. B. Syzdykova, M. P. Belov, I. A. Abrikosov, Thermodynamic properties of tin: Part i experimental investigation, abinitio modelling of -, -phase and a thermodynamic description for pure metal in solid and liquid state from 0 k, Calphad 65 (2019) 50–72.

C. Li, P. Wu, Correlation of bulk modulus and the constituent element properties of binary intermetallic compounds, Chemistry of Materials 13 (12) (2001) 4642–4648.

X. Shen, Q. Sun, J. Zhu, Y. Yao, J. Liu, C. Jin, R. Yu, R. Wang, Structural

stability and Raman scattering of CoPt and NiPt hollow nanospheres under high pressure, Progress in Natural Science: Materials International 23 (4) (2013) 382–387.

Table 1

Conditions used during the synthesis of $Pt(Cu_{0.67}Sn_{0.33})$ and the products obtained.

Synthesis	Temperature [a]	Obtained phases - Le Bail / Å	Reported phases / Å
Elements	Ambient	Pt ($a = 3.9187(1)$, $Fm\bar{3}m$)	Pt ($a = 3.9156$, ICSD-241774)
		Cu ($a = 3.6158(1)$, $Fm\bar{3}m$)	Cu ($a = 3.6149$, ICSD-627114)
		β-Sn ($a = 5.8324(1)$, $c = 3.1819(1)$, $I41/amd$)	β-Sn ($a = 5.8313$, $c = 3.1814$, ICSD-52269)
S1	573 K	Pt ($a = 3.9151(4)$, $Fm\bar{3}m$)	Pt ($a = 3.9156$, ICSD-241774)
		Sn ($a = 3.2846(7)$, $Im\bar{3}m$)	Sn ($a = 3.287$, ICDD-01-073-6846)
		$PtSn_2$ ($a = 6.4238(8)$, $Fm\bar{3}m$)	$PtSn_2$ ($a = 6.422$, ICDD-00-007-0371)
		Pt_2Sn_3 ($a = 4.3418(9)$, $c = 12.971(2)$, $P63/mmc$)	Pt_2Sn_3 ($a = 4.334$, $c = 12.96$, ICDD-03-065-3553)
		PtSn ($a = 4.073(1)$, $c = 5.460(2)$, $P63/mmc$)	PtSn ($a = 4.100$, $c = 5.432$, ICDD-00-025-0614)
		PtCu ($a = 3.7986(5)$, $Fm\bar{3}m$)	PtCu ($a = 3.796$, ICDD-00-048-1549)
		γ-Cu_3Sn ($a = 6.206(1)$, $F\bar{4}3m$)	γ-Cu_3Sn ($a = 6.2156$, ICSD-185003)
		η-Cu_6Sn_5 ($a = 4.2498(8)$, $c = 5.0698(8)$, $P63/mmc$)	η-Cu_6Sn_5 ($a = 4.2062$, $c = 5.0974$, ICDD-00-047-1575)

[a] 6 K/min heating rate. After keeping the sample for 10 h at the highest temperature the furnace was switched off and the pellet was cooled down to ambient conditions in the furnace within 12 h.

Table 2

Conditions used during the synthesis of $Pt(Cu_{0.67}Sn_{0.33})$ and the products obtained.

Synthesis	Temperature [a,b]	Obtained phases - Le Bail / Å	Reported phases / Å
S2	523 K - 773 K	$Pt(Cu_{0.67}Sn_{0.33})$ (a = 2.8194(5), c = 3.6668(8), $P4/mmm$)	-
		PtCu (a = 3.879(1), $Fm\bar{3}m$)	PtCu (a = 3.796, ICDD-00-048-1549)
S3	1023 K	$Pt(Cu_{0.67}Sn_{0.33})$ (a = 2.8244(1), c = 3.6198(1), $P4/mmm$)	-
		PtCu (a = 3.8026(2), $Fm\bar{3}m$)	PtCu (a = 3.796, ICDD-00-048-1549)
		Pt_3Sn (a = 3.9875(1), $Pm\bar{3}m$)	Pt_3Sn (a = 4.0, ICDD-01-072-2978)
		η'-Cu_5Sn_4 (a = 10.1016(3), b = 7.1896(2), c = 9.8058(2), β=62.518(1)°, $P21/c$)	η'-Cu_5Sn_4 (a = 9.83, b = 7.27, c = 9.83, β=62.5°, ICSD-150125)
S4	523 K - 1023 K	$Pt(Cu_{0.67}Sn_{0.33})$ (a = 2.8220(1), c = 3.6363(1), $P4/mmm$)	-
		η'-Cu_5Sn_4 (a = 10.1209(3), b = 7.1995(2), c = 9.8125(3), β=62.396(2)°, $P21/c$)	η'-Cu_5Sn_4 (a = 10.1209(3), b = 7.1995(2), c = 9.8125(3)
S5	523 K - 1023 K Quenched	$Pt(Cu_{0.67}Sn_{0.33})$ (a = 2.8211(1), c = 3.6489(1), $P4/mmm$)	-
S6	523 K - 1023 K Quenched	$Pt(Cu_{0.67}Sn_{0.33})$ (a = 2.8256(1), c = 3.6258(1), $P4/mmm$)	-

[a] 6 K/min heating rate. After 10 h at the highest temperature the furnace was switched off and the pellet was cooled down to ambient conditions in the furnace within 12 h. Compressed air was used for temperature-quenching the samples after taking them out of the furnace.

[b] In those syntheses where two temperatures are given, the sample was kept at the initial annealing temperature for 5 h, and then was kept at the second temperature for 10 h.

Table 3

Arc-Melter synthesis of $Pt(Cu_{0.67}Sn_{0.33})$ and the products obtained.

Synthesis	Obtained phases - Le Bail / Å	Reported phases / Å
S7	$Pt(Cu_{0.67}Sn_{0.33})$ (a = 2.8290(2), c = 3.6570(2), $P4/mmm$)	-
	$Pt_{0.9}Sn_{0.1}$ (a = 3.9566(5), $Fm\bar{3}m$)	$Pt_{0.9}Sn_{0.1}$ (a = 3.9416, ICSD-105797)
S7-annealed [a]	$Pt(Cu_{0.67}Sn_{0.33})$ (a = 2.83100(4), c = 3.64482(5), $P4/mmm$)	-
	$Pt(Cu_{0.67}Sn_{0.33})$ (a = 2.83355(4), c = 3.64972(5), $P4/mmm$)	-
	$Pt(Cu_{0.67}Sn_{0.33})$ (a = 2.8369(1), b = 2.8476(1), c = 3.6556(1), $Pmmm$)	-
	$Pt_{0.92}Sn_{0.08}$ (a = 3.9827(1), $Fm\bar{3}m$)	$Pt_{0.9}Sn_{0.1}$ (a = 3.9416, ICSD-105797)

[a] The annealing was done using a 1.3 K/min heating rate up to 973 K where it was keep for 144 h. After the isotherm time was completed, the furnace was switched off and the pellet was cooled down a ambient conditions in the furnace within 12 h.

Table 4

Lattice parameters of $Pt(Cu_{0.67}Sn_{0.33})$ from Rietveld refinement and from DFT.

Lattice Parameters [a]	S5	S6	DFT [b]
a / Å	2.82101(3)	2.8262(1)	2.8762
c / Å	3.64874(6)	3.6248(1)	3.6984
V / Å^3	29.037(1)	28.953(1)	30.56

[a] Density from X-ray diffraction: 15.976 g/cm^3 (S5) and 15.945 g/cm^3 (S6) .

[b] The DFT values are $\frac{1}{3}$ of the supercell used in all the calculations. The angles of the supercell deviated by $<0.1°$ from 90° after the geometry optimization.

Table 5

$Pt(Cu_{0.67}Sn_{0.33})$ crystal structure obtained by Rietveld refinement and reliability factors. Space Group $P4/mmm$.

S5 - λ = 1.5406Å						
Atom	Wyckoff position	x/a	y/b	z/c	B / Å^2	Occupation
Pt	1a	0	0	0	0.20(2)	1.0
Cu / Sn	1d	0.5	0.5	0.5	0.41(3)	0.68(1) / 0.32(1)
χ^2	R_p	R_{wp}	R_{exp}	R_f	data points	independent parameters
11.6	8.64	13.5	3.95	8.67	6855	10
S6 - λ = 0.1204Å						
Atom	Wyckoff position	x/a	y/b	z/c	B / Å^2	Occupation
Pt	1a	0	0	0	0.58(4)	1.0
Cu / Sn	1d	0.5	0.5	0.5	0.63(9)	0.648(5) / 0.352(5)
χ^2	R_p	R_{wp}	R_{exp}	R_f	data points	independent parameters
5.57	3.43	8.82	2.13	2.62	2877	8

Table 6

Heat capacity data were fitted in three different temperature ranges using fifth-order polynomial functions $Cp(T) = a_0 + a_1 \times T a_2 \times T^2 a_3 \times T^3 + a_4 \times T^4 + a_5 \times T^5$

T range	a_0	a_1	a_2	a_3	a_4	a_5
393 K - 50 K	-21.132	1.1119	-0.0075682	2.7352e-05	-4.9738e-08	3.6051e-11
50 K - 10 K	1.1308	-0.246	0.015998	0.00015861	-8.1091e-06	6.6106e-08
10 K - 3.8 K	-0.027122	0.027553	-0.0072684	0.0012926	-7.0547e-05	2.3771e-06

Table 7

Bulk modulus of $Pt(Cu_{0.67}Sn_{0.33})$ using 2^{nd}-order Birch-Murnaghan equation of state.

	x_0 / Å or Å^3	B_0 / GPa	B'
a	2.829(2)	239(9)	4
c	3.627(3)	193(7)	4
V	29.02(7)	222(8)	4
V (DFT, random)	30.42(6)	200(5)	4
V (DFT, SQS)	30.57(8)	189(8)	4

Table 8

Bulk modulus of $Pt(Cu_{0.67}Sn_{0.33})$ using 3^{rd}-order Birch-Murnaghan equation of state.

	x_0 / Å or Å^3	B_0 / GPa	B'
a	2.830(3)	222(29)	5(2)
c	3.626(4)	201(23)	3(1)
V	29.03(9)	215(27)	5(2)
V (DFT, random)	30.49(9)	179(18)	5(1)
V (DFT, SQS)	30.6(1)	174(28)	5(2)